


Article

Correction of Flow Curves and Constitutive Modelling of a Ti-6Al-4V Alloy

Ming Hu ^{1,2} , Limin Dong ^{2,*}, Zhiqiang Zhang ², Xiaofei Lei ², Rui Yang ² and Yuhui Sha ¹

¹ School of Materials Science and Engineering, Northeastern University, 3 Wenhua Road, Shenyang 110819, China; mhu13s@imr.ac.cn (M.H.); yhsha@mail.neu.edu.cn (Y.S.)

² Institute of Metal Research, Chinese Academy of Sciences, 72 Wenhua Road, Shenyang 110016, China; zqzhang@imr.ac.cn (Z.Z.); xflel@imr.ac.cn (X.L.); ryang@imr.ac.cn (R.Y.)

* Correspondence: lmdong@imr.ac.cn; Tel.: +86-242-397-1942

Received: 9 March 2018; Accepted: 5 April 2018; Published: 10 April 2018



Abstract: Isothermal uniaxial compressions of a Ti-6Al-4V alloy were carried out in the temperature range of 800–1050 °C and strain rate range of 0.001–1 s⁻¹. The effects of friction between the specimen and anvils as well as the increase in temperature caused by the high strain rate deformation were considered, and flow curves were corrected as a result. Constitutive models were discussed based on the corrected flow curves. The correlation coefficient and average absolute relative error for the strain compensated Arrhenius-type constitutive model are 0.986 and 9.168%, respectively, while the values for a modified Johnson-Cook constitutive model are 0.924 and 22.673%, respectively. Therefore, the strain compensated Arrhenius-type constitutive model has a better prediction capability than a modified Johnson-Cook constitutive model.

Keywords: Ti-6Al-4V alloy; isothermal compression test; correction of flow curves; constitutive model

1. Introduction

Hot working plays an important role in the production of materials with required shape, microstructure, and mechanical properties [1]. However, the flow behaviors of metals and alloys during hot working processing are complex and can be affected by many factors, such as temperature, strain, and strain rate, etc. [2,3]. Understanding the flow behaviors of metals and alloys at high temperatures is of great importance for designers working on metal thermo-mechanical processing [4,5]. Nowadays, the finite element method (FEM) has been extensively applied in the scope of engineering, due to its advantages of lower costs, time-consuming to understand materials formability, and optimal processing parameters [6]. The accuracy of FEM results depends on the veracity of the constitutive model [7].

Most experimental data of constitutive models are based on isothermal compression tests [8,9]. During compression processing, adiabatic heating and interfacial friction between the specimen and anvils have great influences on the mechanical responses of the materials [10]. However, in this study the effects of these two factors on the flow stress-strain curve in the Thermal/Mechanical Simulator were not considered. They may bring out an uncertain error of flow stress between test and actual values.

Constitutive models mainly include a phenomenological constitutive model, a physical based constitutive model, and an artificial neural network (ANN) [11]. Phenomenological constitutive models are widely used to simulate the plastic forming processes of metals and alloys [11]. Among these phenomenological constitutive models, the Johnson-Cook model [12] and Arrhenius-type model [13] are extensively used in metals and alloys to describe the relationships between the flow stress, strain rate, and temperature. The Johnson-Cook model assumes that strain hardening, strain rate hardening, and thermal softening are three independent phenomena that can be isolated from each other [11].

The coupled effects of temperatures, strain rates, and strain on the flow behaviors of alloys were omitted [14]. A modified Johnson-Cook model was proposed by Lin [15] to overcome these drawbacks, and has been successfully applied to predict the flow stress in 20CrMo [8], titanium matrix composites (TiCp/Ti) [16], and Co-27Cr-5Mo alloy [17], etc. An Arrhenius-type model was applied to hot working by Sellars and Tegart. In this model, hot working was considered to be a thermally activated process, which can be described by strain rate equations similar to those employed in creep studies [18]. Meanwhile, this model has the advantages of simplicity and applicability, thus it has been widely used. However, the effect of strain was not considered in the Arrhenius-type model. In fact, strain has a significant influence on flow behaviors during hot working processing. Thus, a modified Arrhenius model considering the compensation of strain was proposed to predict the flow stress in 42CrMo steel [19], Ti-6242s [9], Ti-6Al-4V [20], Ti-6Al-7Nb [21], and 7050 aluminum alloy [22], etc.

Ti-6Al-4V alloy is an $\alpha + \beta$ type dual-phase titanium alloy which has been widely used in the aerospace industry due to its excellent properties, such as low density, high specific strength, and good corrosion resistance [23]. However, the hot deformation of the Ti-6Al-4V alloy is a difficult process in controlling microstructure and mechanical properties, due to its narrow processing window of temperature and time [24]. Therefore, it is very important to comprehensively consider the influences of various factors (such as friction, temperature increasing, strain, strain rate, and temperature, etc.) on its flow behaviors. The objective of this study is to establish the suitable constitutive model to predict the high temperature flow behaviors of Ti-6Al-4V alloy. To this end, isothermal hot compression tests were conducted over a wide range of temperatures and strain rates. The flow curves were corrected by considering the effects of friction and temperature increasing. And then, the modified Johnson-Cook model and strain compensated Arrhenius-type constitutive model are used to investigate the alloy's flow behaviors. Finally, the correlation coefficient and average absolute relative error are used to examine the validity of the constitutive equations over the entire range of temperatures and strain rates and the prediction capability between the two constitutive models is compared.

2. Experimental Procedure and Corrected Approach

2.1. Experimental Procedure

The material used in this study is a hot-rolled and annealed Ti-6Al-4V bar with a chemical composition (wt %): 6.2Al, 4.6V and Ti balance. The β transus temperature of the present alloy is about 995 °C tested by metallographic method. The starting microstructure is given in Figure 1. As shown, the microstructure consists of equiaxed primary α phase and retained β .

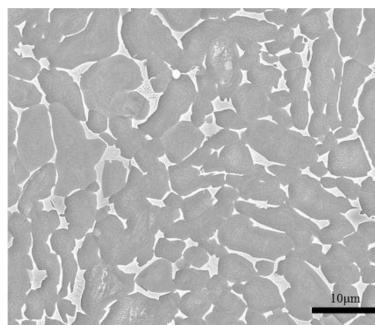


Figure 1. Starting microstructure of the Ti-6Al-4V alloy.

The cylindrical specimens were machined in a diameter of 8 mm and a height of 12 mm. Isothermal uniaxial hot compression tests were conducted on a Gleeble-3500 Thermal/Mechanical Simulator (Dynamic Systems Inc., New York, NY, USA). A thin layer of graphite was used to minimize friction between the specimen and the anvils. The deformation temperature ranges from 800 °C to 1050 °C at

an interval of 50 °C. The strain rates were 0.001 s⁻¹, 0.01 s⁻¹, 0.1 s⁻¹, and 1 s⁻¹. The specimens were deformed up to total true strain of 0.9.

2.2. Friction and Temperature Corrected Approach

Although graphite was used to lubricate the contacting surface, the friction coefficient at high temperatures cannot be lowered to a negligible level [10]. The friction corrected flow stress can be calculated using the following equations [25]:

$$\sigma = \frac{\sigma_0 C^2}{2[\exp(C) - C - 1]}, \quad (1)$$

$$C = 2mR/h, \quad (2)$$

$$R = R_0 \sqrt{\frac{h_0}{h}}, \quad (3)$$

$$m = \frac{(R/h)b}{\left(\frac{4}{\sqrt{3}}\right) - \left(\frac{2b}{3\sqrt{3}}\right)}, \quad (4)$$

where σ is the friction corrected flow stress, σ_0 is the tested flow stress, R_0 and h_0 are initial radius and height of specimen, R and h are instantaneous radius and height of specimen, m is the friction coefficient that is determined according to the amount of barreling for each specimen [25]. Specifically, the barreling factor b is calculated as follows:

$$b = 4 \frac{\Delta R}{R} \frac{h}{\Delta h}, \quad (5)$$

$$\Delta R = R_M - R_T, \quad (6)$$

where ΔR is the difference between the maximum and minimum radius of the specimen, R_M is maximum radius, R_T is minimum radius, Δh is the difference between initial and final heights of the sample.

R_T can be calculated using the following equation [26]:

$$R_T = \sqrt{3 \frac{h_0}{h} R_0^2 - 2R_M^2}. \quad (7)$$

Temperature will rise during hot compression process. The tested flow stress is not the flow stress under designated temperature. The difference between the designated and tested flow stress $\Delta\sigma$ can be calculated using the following equation [27]:

$$\Delta\sigma = \Delta T \frac{d\sigma}{dT}, \quad (8)$$

where ΔT is the difference between the actual and designated temperature.

3. Results and Discussion

3.1. Corrected Flow Curves by Considering the Effect of Friction and Temperature Increasing

In order to quantify the effect of friction factors on the flow behavior of alloy, B. Roebuck [28] defined barreling coefficient B , as shown in Equation (9). Barreling is caused by friction at the test piece interfaces.

$$B = \frac{hR_M^2}{h_0R_0^2}, \quad (9)$$

When $1 < B \leq 1.1$, the difference between the actual and tested flow stress is small. When $B \geq 1.1$, the friction has a great influence on flow stress. Table 1 lists the values of B under different deformation conditions.

Table 1. The values of B under different deformation conditions.

Temperature (°C)	Strain Rate (s ⁻¹)				
	0.001	0.01	0.1	1	10
800	1.23367	1.22045	1.22528	1.24138	1.19697
850	1.24819	1.247	1.24637	1.24822	1.20488
900	1.17906	1.21424	1.24033	1.27114	1.23279
950	1.18657	1.18411	1.18164	1.23693	1.24067
1000	1.16292	1.14611	1.12361	1.13064	1.21576
1050	1.18666	1.16968	1.21577	1.25549	1.16799

Table 1 shows that all of the B values are ≥ 1.1 , so it is needed to revise the tested flow stress by the previous friction corrected approach, and the corrected flow stress of 800 °C is shown in Figure 2a. The tested flow stress is higher than the actual flow stress due to the friction between the specimen and anvil.

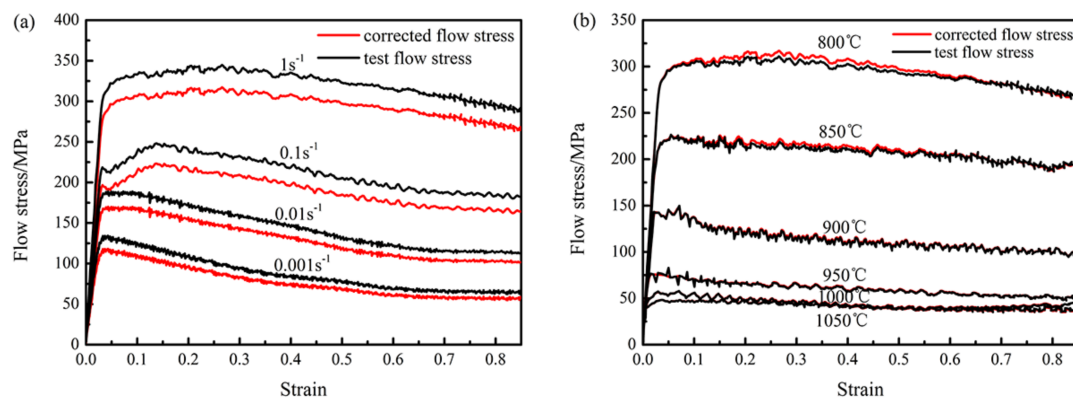


Figure 2. (a) Friction corrected flow stress curves of 800 °C; (b) temperature corrected flow stress curves at strain rate of 1 s⁻¹.

Temperature increasing can be ignored in low strain rate conditions, but it is obvious in high strain rate compression tests. Figure 2b shows the temperature corrected flow stress in a strain rate of 1 s⁻¹. The tested flow stress is lower than the actual flow stress due to the temperature increasing at high strain rate.

Figure 3 shows friction and temperature corrected flow stress curves of isothermally compressed Ti-6Al-4V alloy at different deformation temperatures. The shapes of the stress-strain curves have the same features in 800–900 °C. At strain rate of 1 s⁻¹, the curves are steady-state type. At strain rate slower than 1 s⁻¹, the curves are flow softening. The flow stress curves of 950–1050 °C are similar, but different from 800–900 °C. At strain rate of 1 s⁻¹ and 0.1 s⁻¹, the curves are flow softening. At strain rate of 0.01 s⁻¹ and 0.001 s⁻¹, the curves are steady-state type.

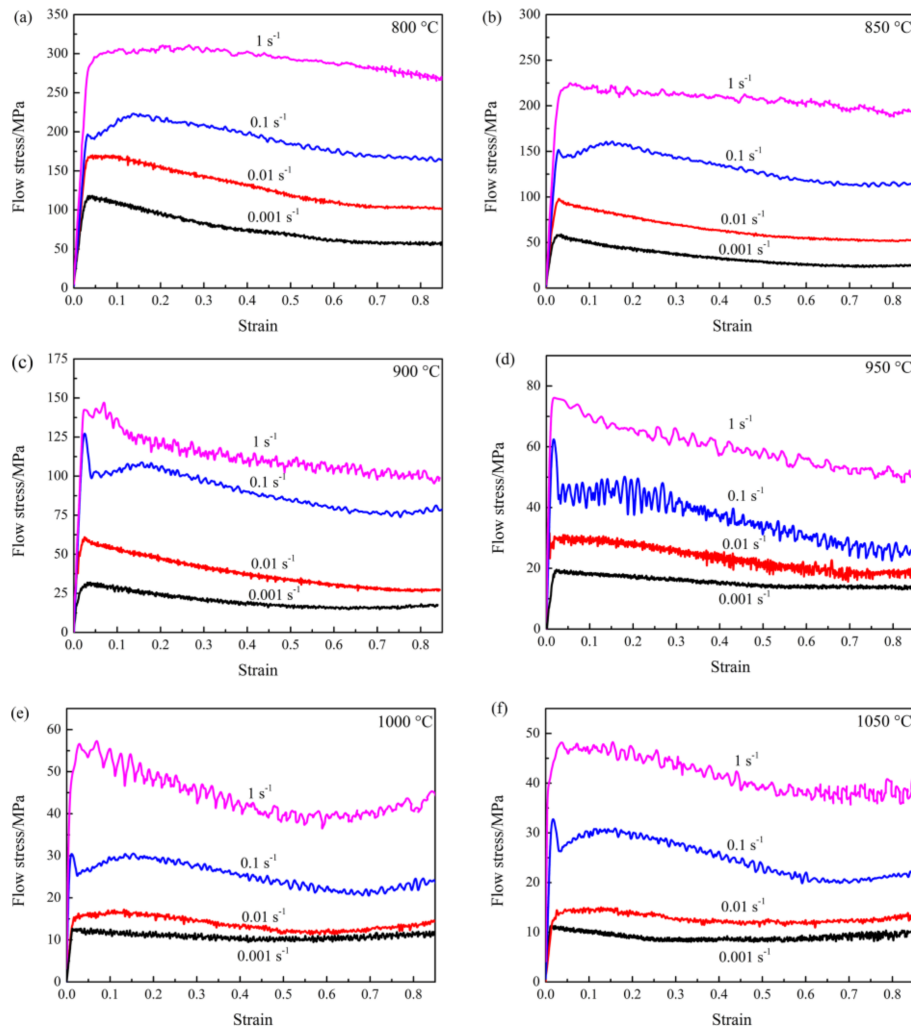


Figure 3. Friction and temperature corrected flow stress curves of isothermally compressed Ti-6Al-4V alloy at different deformation temperatures: (a) 800 °C; (b) 850 °C; (c) 900 °C; (d) 950 °C; (e) 1000 °C; (f) 1050 °C.

3.2. Constitutive Models

Based on the similarity of the flow stress curves, the constitutive models were calculated in 800–900 °C and 950–1050 °C, respectively.

3.2.1. Modified Johnson-Cook Model

The modified Johnson-Cook model can be expressed as follows [15]:

$$\sigma = (A_1 + B_1\varepsilon + B_2\varepsilon^2)(1 + C_1\ln \dot{\varepsilon}^*) \exp[(\lambda_1 + \lambda_2\ln \dot{\varepsilon}^*)(T - T_r)], \quad (10)$$

where σ is flow stress (MPa), ε is the true strain, $\dot{\varepsilon}$ is the strain rate (s^{-1}), $\dot{\varepsilon}_0$ is the reference strain rate (s^{-1}), $\dot{\varepsilon}^* = \dot{\varepsilon}/\dot{\varepsilon}_0$ is the dimensionless strain rate, T is the absolute temperature (K), T_r is the reference temperature, $A_1, B_1, B_2, C_1, \lambda_1, \lambda_2$ are the material constants.

In the range of 800–900 °C, 800 °C and $1 s^{-1}$ are taken as reference temperature (T_r) and strain rate ($\dot{\varepsilon}_0$) to evaluate the material constants. At 800 °C and $1 s^{-1}$, Equation (10) can be written as follows:

$$\sigma = A_1 + B_1\varepsilon + B_2\varepsilon^2, \quad (11)$$

Then, the values of A_1 , B_1 and B_2 can be evaluated by performing a two-order polynomial fitting the relationship between σ and ε , as shown in Figure 4. When the deformation temperature is 800 °C, Equation (10) can be expressed as follows:

$$\frac{\sigma}{A_1 + B_1\varepsilon + B_2\varepsilon^2} = 1 + C_1 \ln \dot{\varepsilon}^*, \quad (12)$$

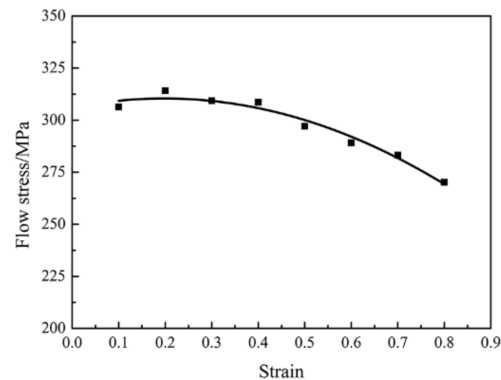


Figure 4. The relationship between stress and strain at 800 °C and 1 s⁻¹.

Substituting the four different strain rates and the corresponding flow stress at different strains into Equation (12), the values of material constant C_1 can be evaluated by linear fitting the relationship between $\sigma/(A_1 + B_1\varepsilon + B_2\varepsilon^2)$ and $\ln \dot{\varepsilon}^*$ (shown in Figure 5).

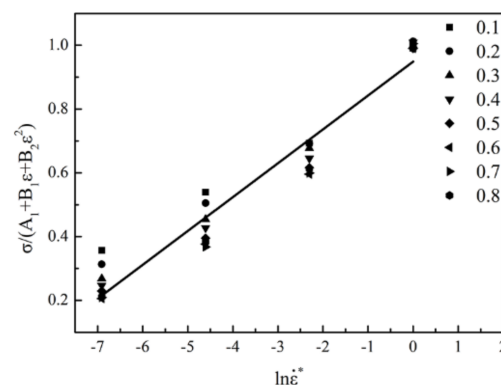


Figure 5. The relationship between stress and strain at 800 °C and 1 s⁻¹. The relationship between $\sigma/(A_1 + B_1\varepsilon + B_2\varepsilon^2)$ and $\ln \dot{\varepsilon}^*$ at 800 °C.

Introducing one new parameter λ , which is equal to $(\lambda_1 + \lambda_2 \ln \dot{\varepsilon}^*)$. Then, Equation (10) can be transformed as follows:

$$\frac{\sigma}{(A_1 + B_1\varepsilon + B_2\varepsilon^2) * (1 + C_1 \ln \dot{\varepsilon}^*)} = \exp[\lambda(T - T_r)], \quad (13)$$

Taking the logarithm of both sides of Equation (13) yields:

$$\ln \left[\frac{\sigma}{(A_1 + B_1\varepsilon + B_2\varepsilon^2) * (1 + C_1 \ln \dot{\varepsilon}^*)} \right] = \lambda(T - T_r), \quad (14)$$

The relationships between $\ln\{\sigma/(A_1 + B_1\varepsilon + B_2\varepsilon^2)(1 + C_1 \ln \dot{\varepsilon}^*)\}$ and $(T - T_r)$ can be obtained at different strain rates, strains and deformation temperatures, as shown in Figure 6. Then, λ_1 and λ_2 can be calculated by linear fitting $\lambda - \ln \dot{\varepsilon}^*$. The values of A_1 , B_1 , B_2 , C_1 , λ_1 and λ_2 in 800–900 °C

are calculated by the same procedure. Table 2 lists the values of the parameters of the modified Johnson-Cook model for the Ti-6Al-4V alloy.

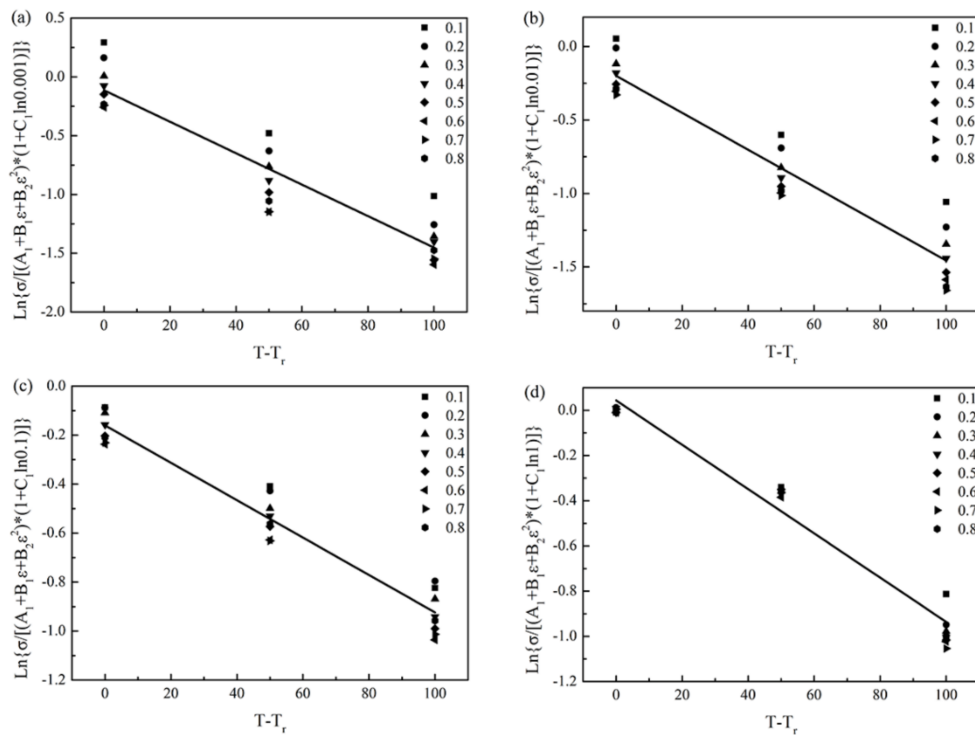


Figure 6. The relationships between $\ln\{\sigma/[(A_1 + B_1 \epsilon + B_2 \epsilon^2)(1 + C_1 \ln \dot{\epsilon}^*)]\}$ and $(T - T_r)$ at different strain rates: (a) 0.001 s^{-1} ; (b) 0.01 s^{-1} ; (c) 0.1 s^{-1} and (d) 1 s^{-1} .

Table 2. The parameters of the modified Johnson-Cook model for Ti-6Al-4V alloy.

	A_1	B_1	B_2	C_1	λ_1	λ_2
800–900 °C	305.9702	44.92423	−113.465	0.10623	−0.00969	0.000551
950–1050 °C	74.03002	−37.8908	11.0537	0.1073	−0.00378	0.000178

Then the modified Johnson-Cook constitutive model for Ti-6Al-4V alloy can be obtained.
800–900 °C:

$$\sigma = (305.9702 + 44.92423\epsilon - 113.465\epsilon^2)(1 + 0.10623 \ln \dot{\epsilon}^*) \exp[(-0.00969 + 0.000551 \ln \dot{\epsilon}^*)(T - T_r)] \quad (15)$$

950–1050 °C:

$$\sigma = (74.03002 - 37.8908\epsilon + 11.0537\epsilon^2)(1 + 0.1073 \ln \dot{\epsilon}^*) \exp[(-0.00378 + 0.000178 \ln \dot{\epsilon}^*)(T - T_r)] \quad (16)$$

Using the modified Johnson-Cook constitutive model, the predicted flow stress was obtained and can be verified through comparing with the experimental data, as shown in Figure 7. It could be observed that the predicted flow stress only has a good agreement with the experimental data at a reference deformation condition and strain rate of 0.001 s^{-1} , but the agreement is not good in other deformation conditions.

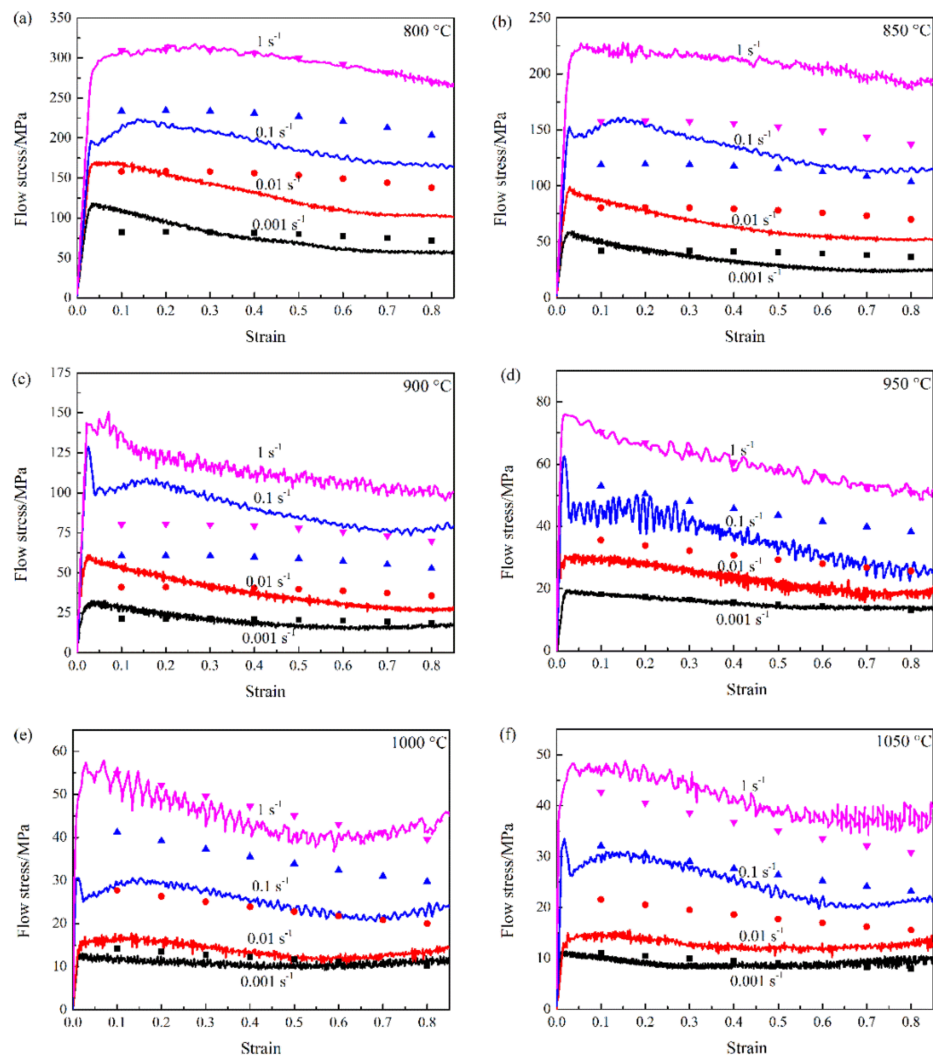


Figure 7. Comparison between the experimental (solid lines) and predicted (dots) flow stress from the modified Johnson-Cook model at the temperature of (a) 800 °C; (b) 850 °C; (c) 900 °C; (d) 950 °C; (e) 1000 °C; (f) 1050 °C.

3.2.2. Strain Compensated Arrhenius-Type Constitutive Model

The Arrhenius-type constitutive model can be represented in Equation (17),

$$\dot{\epsilon} = AF(\sigma) \exp\left(-\frac{Q}{RT}\right), \quad (17)$$

$$F(\sigma) = \begin{cases} \sigma^{n'} & \alpha\sigma < 0.8 \\ \exp(\beta\sigma) & \alpha\sigma > 1.2 \\ [\sinh(\alpha\sigma)]^n & \text{for all } \sigma \end{cases}, \quad (18)$$

where $\dot{\epsilon}$ is the strain rate (s^{-1}), Q is the activation energy of hot deformation ($\text{kJ}\cdot\text{mol}^{-1}$), R is the universal gas constant ($8.3145 \text{ J}\cdot\text{mol}^{-1}\cdot\text{K}^{-1}$), T is the absolute temperature (K), and σ is flow stress (MPa), A , n' , β , α and n are the material constants, $\alpha = \beta/n'$ [29]. The stress multiplier α is an adjustable constant that brings $\alpha\sigma$ into the correct range that gives linear and parallel lines in $\ln\dot{\epsilon}$ versus $\ln\{\sinh(\alpha\sigma)\}$ [30].

However, the effect of strain on flow stress was not considered in Equation (17). In this study, the effects of strain on the material constants of constitutive models were investigated. The strain of 0.6

was taken as an example to illustrate the solution procedures of the material constants. In order to extract β and n' and calculate α , substituting $F(\sigma)$ (low stress values ($\alpha\sigma < 0.8$) and high stress values ($\alpha\sigma > 1.2$)) into Equation (17) respectively:

$$\dot{\epsilon} = B\sigma^{n'}, \quad (19)$$

$$\dot{\epsilon} = C \exp(\beta\sigma), \quad (20)$$

where B and C are the material constants. Taking natural logarithm of both sides of Equations (19) and (20), the following equations can be obtained:

$$\ln(\sigma) = \frac{1}{n'} \ln(\dot{\epsilon}) - \frac{1}{n'} \ln(B), \quad (21)$$

$$\sigma = \frac{1}{\beta} \ln(\dot{\epsilon}) - \frac{1}{\beta} \ln(C). \quad (22)$$

The material constants are independent of the deformed temperatures. Figures 8 and 9 show the relationships between $\ln\sigma$ — $\ln\dot{\epsilon}$ and σ — $\ln\dot{\epsilon}$ for 800–900 °C and 950–1050 °C, respectively. The values of n' and β can be obtained from the mean slope values of $\ln\sigma$ — $\ln\dot{\epsilon}$ and σ — $\ln\dot{\epsilon}$ plots, respectively. For 800–900 °C, the mean value of n' and β was calculated to be 3.767 and 0.0477, respectively. For 950–1050 °C, the mean value of n' and β was calculated to be 4.743 and 0.212, respectively. Then α values were calculated to be 0.0127 (800–900 °C) and 0.0447 (950–1050 °C).

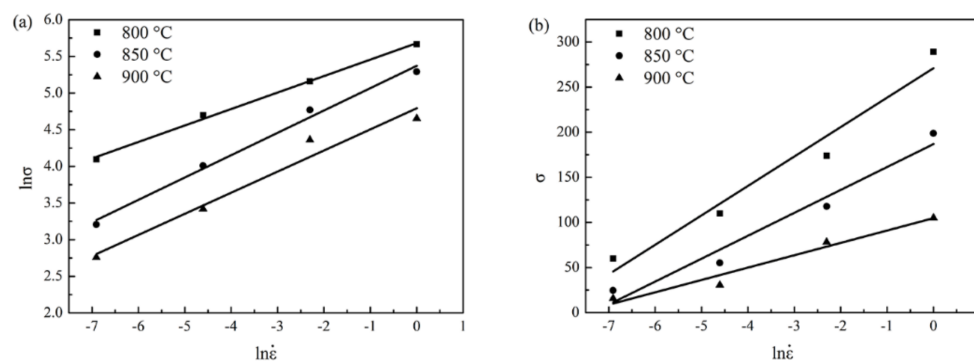


Figure 8. The relationship between (a) $\ln\sigma$ — $\ln\dot{\epsilon}$ and (b) σ — $\ln\dot{\epsilon}$ in 800–900 °C.

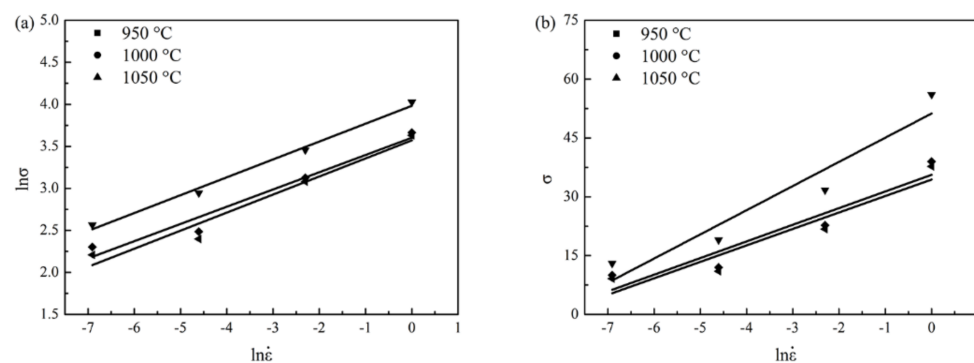


Figure 9. The relationship between (a) $\ln\sigma$ — $\ln\dot{\epsilon}$ and (b) σ — $\ln\dot{\epsilon}$ in 950–1050 °C.

For all the stress levels, Equation (17) can be represented as the following formula:

$$\dot{\epsilon} = A[\sinh(\alpha\sigma)]^n \exp\left(-\frac{Q}{RT}\right), \quad (23)$$

Taking the natural logarithm and transposing from both sides of the Equation (23) yields:

$$\ln[\sinh(\alpha\sigma)] = \frac{\ln \dot{\epsilon}}{n} + \frac{Q}{nRT} - \frac{\ln A}{n}, \quad (24)$$

Figure 10 shows the relationship between $\ln[\sinh(\alpha\sigma)]$ and $\ln \dot{\epsilon}$. The $\ln[\sinh(\alpha\sigma)]$ — $\ln \dot{\epsilon}$ shows a linear relationship. And the slope is $1/n$. The $\ln A$ can also be acquired from Equation (24).

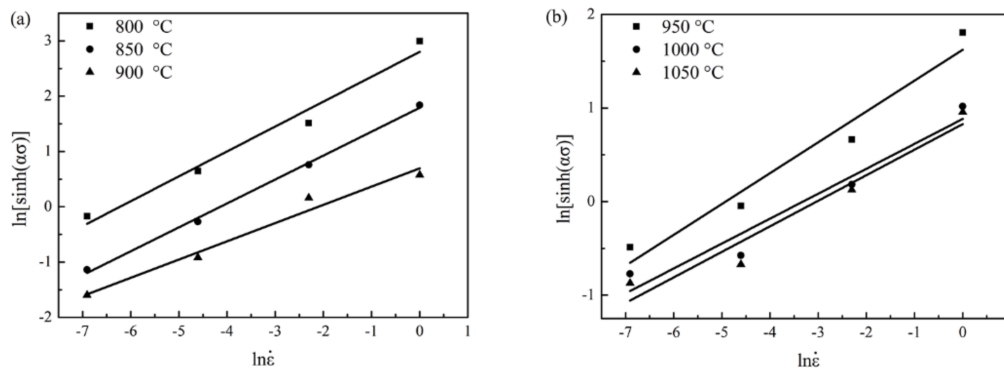


Figure 10. The relationship between $\ln[\sinh(\alpha\sigma)]$ — $\ln \dot{\epsilon}$ for (a) 800–900 °C and (b) 950–1050 °C.

For a particular strain rate, differentiating Equation (24) yields:

$$Q = Rn \frac{d\{\ln[\sinh(\alpha\sigma)]\}}{d(1/T)}, \quad (25)$$

Figure 11 shows the relationship between $\ln[\sinh(\alpha\sigma)]$ and $1000/T$. The value of Q can be derived from the slope and Equation (25). Then Q values were calculated to be $438.39 \text{ kJ}\cdot\text{mol}^{-1}$ (800–900 °C) and $280.64 \text{ kJ}\cdot\text{mol}^{-1}$ (950–1050 °C).

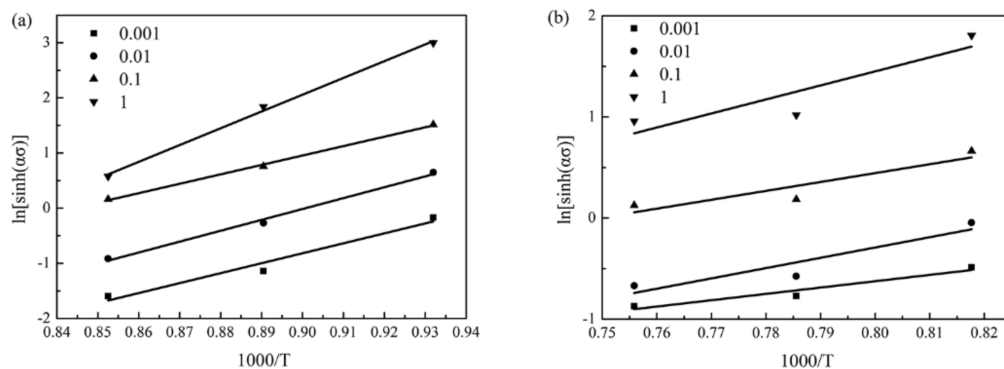


Figure 11. The relationship between $\ln[\sinh(\alpha\sigma)]$ — $1000/T$ for (a) 800–900 °C and (b) 950–1050 °C.

Much of the literature has shown that the activation energy Q and material constants (α , n , A) are influenced by strain [9,20]. Hence, compensation of strain should be considered to derive a precise constitutive model to predict the flow stress. And the influence of strain on the constitutive model is incorporated by assuming that α , n , Q , and $\ln A$ are polynomial functions of strain [31]. In this study, the values of α , n , Q , $\ln A$ were calculated by the same procedure under different deformation strains within the range of 0.1–0.8 with regular interval of 0.1. The influence of strain on material constants

fitted well with a fifth order polynomial, as shown in Figure 12. The coefficients of the polynomial are given in Table 3 (800–900 °C) and Table 4 (950–1050 °C).

$$\begin{aligned} \alpha &= D_0 + D_1\varepsilon + D_2\varepsilon^2 + D_3\varepsilon^3 + D_4\varepsilon^4 + D_5\varepsilon^5 \\ n &= E_0 + E_1\varepsilon + E_2\varepsilon^2 + E_3\varepsilon^3 + E_4\varepsilon^4 + E_5\varepsilon^5 \\ Q &= F_0 + F_1\varepsilon + F_2\varepsilon^2 + F_3\varepsilon^3 + F_4\varepsilon^4 + F_5\varepsilon^5 \\ \ln A &= H_0 + H_1\varepsilon + H_2\varepsilon^2 + H_3\varepsilon^3 + H_4\varepsilon^4 + H_5\varepsilon^5 \end{aligned} \quad (26)$$

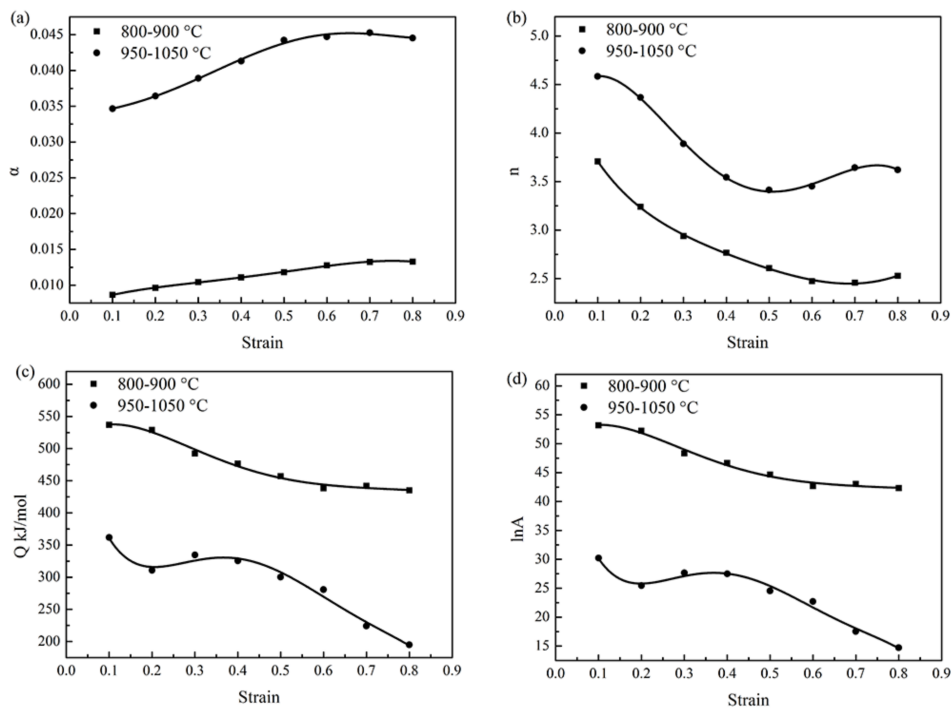


Figure 12. Variation of (a) α , (b) n , (c) Q and (d) $\ln A$ with ε .

Table 3. Polynomial coefficients for α , n , Q , $\ln A$ for 800–900 °C.

α	n	Q	$\ln A$
$D_0 = 0.00694$	$E_0 = 4.59468$	$F_0 = 506.4186$	$H_0 = 50.30346$
$D_1 = 0.02219$	$E_1 = -11.8426$	$F_1 = 656.7189$	$H_1 = 64.77531$
$D_2 = -0.06088$	$E_2 = 35.76194$	$F_2 = -4249.11$	$H_2 = -434.195$
$D_3 = 0.09974$	$E_3 = -63.4781$	$F_3 = 8640.985$	$H_3 = 894.9239$
$D_4 = -0.05019$	$E_4 = 55.43269$	$F_4 = -7629.24$	$H_4 = -800.436$
$D_5 = -0.00901$	$E_5 = -17.3419$	$F_5 = 2514.97$	$H_5 = 267.9284$

Table 4. Polynomial coefficients for α , n , Q , $\ln A$ for 950–1050 °C.

α	n	Q	$\ln A$
$D_0 = 0.03364$	$E_0 = 4.09854$	$F_0 = 584.4601$	$H_0 = 53.59972$
$D_1 = 0.00887$	$E_1 = 10.5984$	$F_1 = -3732.22$	$H_1 = -396.407$
$D_2 = -0.00285$	$E_2 = -69.7254$	$F_2 = 18,715.89$	$H_2 = 2033.636$
$D_3 = 0.22163$	$E_3 = 133.9525$	$F_3 = -41438.3$	$H_3 = -4591.96$
$D_4 = -0.4681$	$E_4 = -92.761$	$F_4 = 41,030.41$	$H_4 = 4648.483$
$D_5 = 0.25605$	$E_5 = 15.50738$	$F_5 = -15175.7$	$H_5 = -1758.81$

By combining the Equations (24) and (27) with the calculated material constants, the constitutive model can be represented as shown in Equation (28)

$$Z = \dot{\epsilon} \exp\left(\frac{Q}{RT}\right), \quad (27)$$

$$\sigma = \frac{1}{\alpha} \ln \left\{ \left(\frac{Z}{A}\right)^{1/n} + \left[\left(\frac{Z}{A}\right)^{2/n} + 1 \right]^{1/2} \right\}, \quad (28)$$

Using the strain compensated constitutive model, the predicted flow stress was obtained and can be verified through comparing with the experimental data, as shown in Figure 13. It could be observed that the predicted flow stress has a good agreement with the experimental data in most of the deformation conditions.

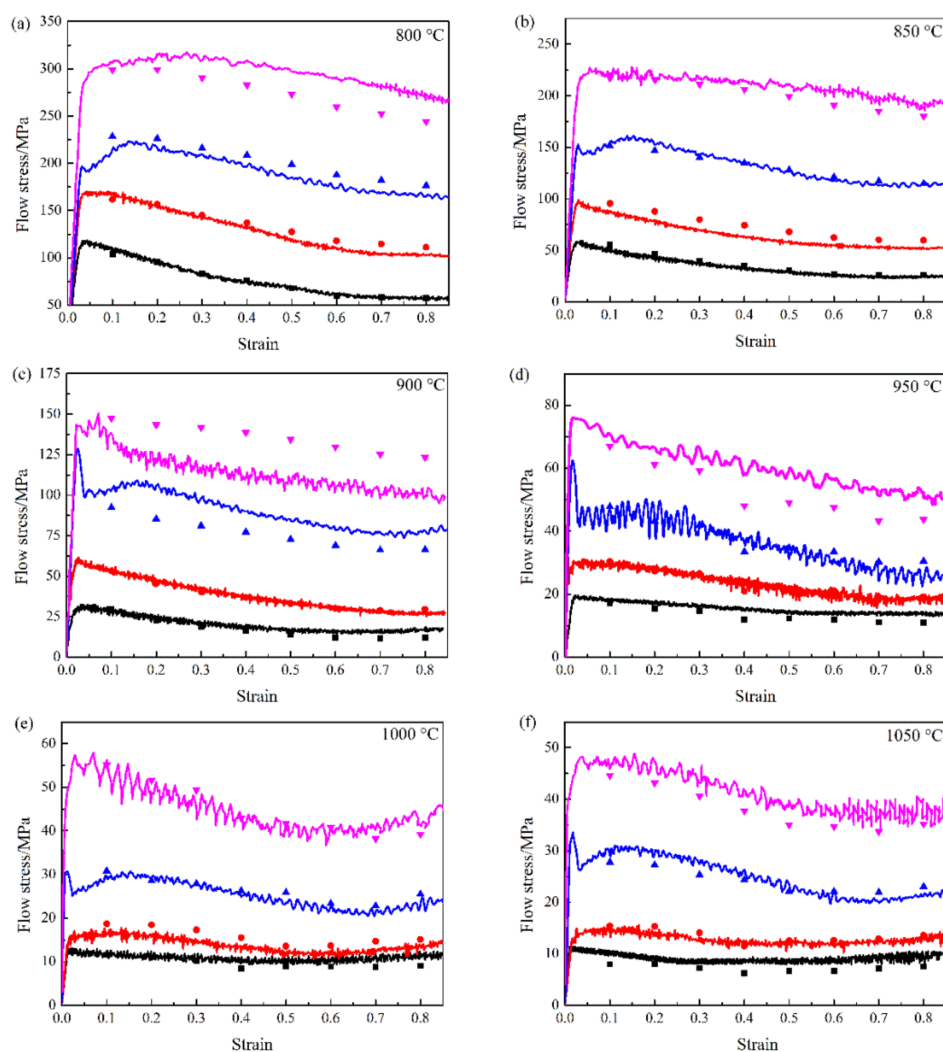


Figure 13. Comparison between the experimental (solid lines) and predicted (dots) flow stress at the temperature of (a) 800 °C; (b) 850 °C; (c) 900 °C; (d) 950 °C; (e) 1000 °C; (f) 1050 °C.

3.3. Formatting of Mathematical Components

In this study, correlation coefficient (R) and average absolute relative error (AARE) were selected as standard statistical parameters to quantify the predictability of the modified Johnson–Cook constitutive model and the strain compensated Arrhenius-type constitutive model. These are expressed as follows:

$$R = \frac{\sum_{i=1}^N (E_i - \bar{E})(P_i - \bar{P})}{\sqrt{\sum_{i=1}^N (E_i - \bar{E})^2 \sum_{i=1}^N (P_i - \bar{P})^2}}, \quad (29)$$

$$\text{AARE}(\%) = \frac{1}{N} \sum_{i=1}^N \left| \frac{E_i - P_i}{E_i} \right|, \quad (30)$$

where E is the experimental flow stress, P is the predicted flow stress derived from the strain compensated constitutive equation. \bar{E} and \bar{P} are the mean values of E and P , respectively. N is the total number of data used in this study. The correlation coefficient R is used to reflect the strength of the linear relationship between the experimental and predicted data. The AARE is calculated in comparison of the relative error and used for determining the predictability of the equation [32]. When $R = 1$ and $\text{AARE} = 0\%$, the predicted data and experimental data are the same. The values of R and AARE of the modified Johnson–Cook constitutive model are 0.924 and 22.673%, as shown in Figure 14a. The values of R and AARE of the strain compensated Arrhenius-type constitutive model are 0.986 and 9.168%, as shown in Figure 14b. The main reason is the predicted flow stress of the modified Johnson–Cook constitutive model was calculated on the basis of the reference deformation condition. The predicted flow stress fit well at the reference deformation condition. The values of C_1 , λ_1 and λ_2 were calculated by linear fitting. But the linear relationship is not a very good in some deformation conditions. The values of α , n , Q , $\ln A$ of the strain compensated Arrhenius-type constitutive model were calculated by linear fitting under different deformation strains. The linear relationship is good in most of the deformation conditions. The results reveal that the strain compensated Arrhenius-type constitutive model is better suited for predicting the flow stress of a Ti-6Al-4V alloy than the modified Johnson–Cook constitutive model.

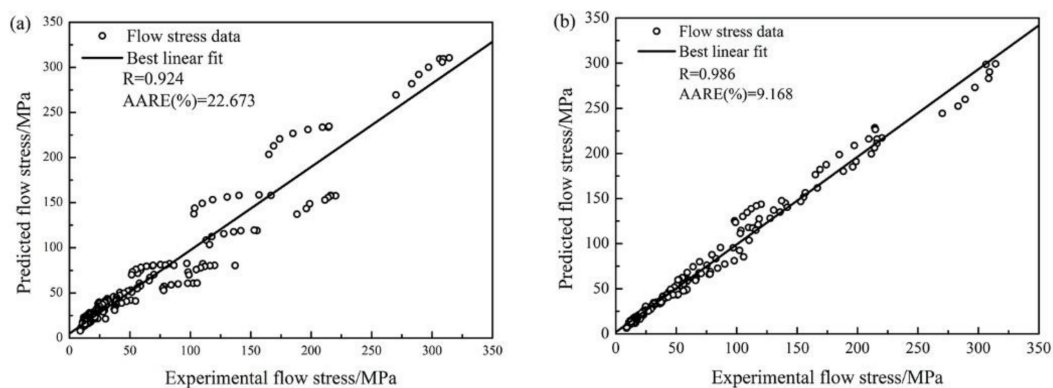


Figure 14. Correlation between the experimental and predicted flow stress data (a) the modified Johnson–Cook constitutive model; (b) the strain compensated Arrhenius-type constitutive model.

4. Conclusions

Isothermal compressions of Ti-6Al-4V alloy were carried out in the temperature range of 800–1050 °C and strain rate range of 0.001–1 s⁻¹, and constitutive analysis of the alloy was conducted. The following conclusions can be drawn from this study:

- (1) The barreling coefficient B values are ≥ 1.1 in all temperatures and strain rates, which shows that friction has a significant influence on flow stress. The friction can result in a tested flow stress that is higher than the actual flow stress, while the temperature increasing is in contrast.
- (2) Based on the similarity of the flow stress curves, the constitutive model should be calculated in 800–900 °C and 950–1050 °C, separately.
- (3) The modified Johnson–Cook constitutive model only has a good agreement with the experimental data at reference deformation condition and strain rate of 0.001 s^{-1} . But the agreement is not good with other deformation conditions. The correlation coefficient and average absolute relative error for the modified Johnson–Cook constitutive model are 0.924 and 22.673%.
- (4) The strain compensated Arrhenius-type constitutive model has a good agreement with the experimental data in most of the deformation conditions. The correlation coefficient and average absolute relative error for the strain compensated Arrhenius-type constitutive model are 0.986 and 9.168%. Thus, the strain compensated Arrhenius-type constitutive model has a better prediction capability than the modified Johnson–Cook constitutive.

Author Contributions: Ming Hu and Limin Dong conceived and designed the experiments; Ming Hu performed the experiments; Ming Hu, Limin Dong, Zhiqiang Zhang, Xiaofei Lei, and Rui Yang analyzed the data. Yuhui Sha did the revision and direction.

Conflicts of Interest: The authors declare no conflict of interest.

References

1. Mirzadeh, H. Constitutive modeling and prediction of hot deformation flow stress under dynamic recrystallization conditions. *Mech. Mater.* **2015**, *85*, 66–79. [[CrossRef](#)]
2. Gao, P.; Zhan, M.; Fan, X.; Lei, Z.; Cai, Y. Hot deformation behavior and microstructure evolution of TA15 titanium alloy with nonuniform microstructure. *Mater. Sci. Eng. A* **2017**, *689*, 243–251. [[CrossRef](#)]
3. Mosleh, A.; Mikhaylovskaya, A.; Kotov, A.; Pourcelot, T.; Aksenov, S.; Kwame, J.; Portnoy, V. Modelling of the superplastic deformation of the near-alpha titanium alloy (Ti-2.5Al-1.8Mn) using Arrhenius-type constitutive model and artificial neural network. *Metals* **2017**, *7*, 568. [[CrossRef](#)]
4. Lin, Y.C.; Chen, M.S.; Zhong, J. Effects of deformation temperatures on stress/strain distribution and microstructural evolution of deformed 42CrMo steel. *Mater. Des.* **2009**, *30*, 908–913. [[CrossRef](#)]
5. Pu, E.; Zheng, W.; Song, Z.; Feng, H.; Dong, H. Hot deformation characterization of nickel-based superalloy UNS10276 through processing map and microstructural studies. *J. Alloys Compd.* **2017**, *694*, 617–631. [[CrossRef](#)]
6. Cai, J.; Wang, K.; Zhai, P.; Li, F.; Yang, J. A modified Johnson–Cook constitutive equation to predict hot deformation behavior of Ti-6Al-4V alloy. *J. Mater. Eng. Perform.* **2015**, *24*, 32–44. [[CrossRef](#)]
7. Jun, H.J.; Lee, K.S.; Kato, H.; Kim, H.S.; Chang, Y.W. Constitutive model for high temperature deformation behavior of Ti-Zr-Ni-Be bulk metallic glass in supercooled liquid region. *Comput. Mater. Sci.* **2012**, *61*, 213–223. [[CrossRef](#)]
8. He, A.; Xie, G.; Zhang, H.; Wang, X. A comparative study on Johnson–Cook, modified Johnson–Cook and Arrhenius-type constitutive models to predict the high temperature flow stress in 20crmo alloy steel. *Mater. Des.* **2013**, *52*, 677–685. [[CrossRef](#)]
9. Hajari, A.; Morakabati, M.; Abbasi, S.M.; Badri, H. Constitutive modeling for high-temperature flow behavior of Ti-6242s alloy. *Mater. Sci. Eng. A* **2017**, *681*, 103–113. [[CrossRef](#)]
10. Li, Y.; Onodera, E.; Chiba, A. Friction coefficient in hot compression of cylindrical sample. *Mater. Trans.* **2010**, *51*, 1210–1215. [[CrossRef](#)]
11. Lin, Y.C.; Chen, X.M. A critical review of experimental results and constitutive descriptions for metals and alloys in hot working. *Mater. Des.* **2011**, *32*, 1733–1759. [[CrossRef](#)]
12. Tan, J.Q.; Zhan, M.; Liu, S.; Huang, T.; Guo, J.; Yang, H. A modified Johnson–Cook model for tensile flow behaviors of 7050-T7451 aluminum alloy at high strain rates. *Mater. Sci. Eng. A* **2015**, *631*, 214–219. [[CrossRef](#)]
13. Jonas, J.J.; Sellars, C.M.; Tegart, W.J.M. Strength and structure under hot-working conditions. *Int. Mater. Rev.* **1969**, *14*, 1–24. [[CrossRef](#)]

14. Liang, R.Q.; Khan, A.S. A critical review of experimental results and constitutive models for BCC and FCC metals over a wide range of strain rates and temperatures. *Int. J. Plast.* **1999**, *15*, 963–980. [[CrossRef](#)]
15. Lin, Y.C.; Chen, X.M.; Liu, G. A modified Johnson–Cook model for tensile behaviors of typical high-strength alloy steel. *Mater. Sci. Eng. A* **2010**, *527*, 6980–6986. [[CrossRef](#)]
16. Song, W.; Ning, J.; Mao, X.; Tang, H. A modified Johnson–Cook model for titanium matrix composites reinforced with titanium carbide particles at elevated temperatures. *Mater. Sci. Eng. A* **2013**, *576*, 280–289. [[CrossRef](#)]
17. Trimble, D.; Shipley, H.; Lea, L.; Jardine, A.; O'Donnell, G.E. Constitutive analysis of biomedical grade Co-27Cr-5Mo alloy at high strain rates. *Mater. Sci. Eng. A* **2017**, *682*, 466–474. [[CrossRef](#)]
18. Sellars, C.M.; McEgart, W.J. On the mechanism of hot deformation. *Acta Metall.* **1966**, *14*, 1136–1138. [[CrossRef](#)]
19. Lin, Y.C.; Chen, M.S.; Zhong, J. Constitutive modeling for elevated temperature flow behavior of 42CrMo steel. *Comput. Mater. Sci.* **2008**, *42*, 470–477. [[CrossRef](#)]
20. Cai, J.; Li, F.; Liu, T.; Chen, B.; He, M. Constitutive equations for elevated temperature flow stress of Ti-6Al-4V alloy considering the effect of strain. *Mater. Des.* **2011**, *32*, 1144–1151. [[CrossRef](#)]
21. Pilehva, F.; Zarei-Hanzaki, A.; Ghambari, M.; Abedi, H.R. Flow behavior modeling of a Ti-6Al-7Nb biomedical alloy during manufacturing at elevated temperatures. *Mater. Des.* **2013**, *51*, 457–465. [[CrossRef](#)]
22. Li, J.; Li, F.; Cai, J.; Wang, R.; Yuan, Z.; Xue, F. Flow behavior modeling of the 7050 aluminum alloy at elevated temperatures considering the compensation of strain. *Mater. Des.* **2012**, *42*, 369–377. [[CrossRef](#)]
23. Momeni, A.; Abbasi, S.M. Effect of hot working on flow behavior of Ti-6Al-4V alloy in single phase and two phase regions. *Mater. Des.* **2010**, *31*, 3599–3604. [[CrossRef](#)]
24. Souza, P.M.; Beladi, H.; Singh, R.; Rolfe, B.; Hodgson, P.D. Constitutive analysis of hot deformation behavior of a Ti6Al4V alloy using physical based model. *Mater. Sci. Eng. A* **2015**, *648*, 265–273. [[CrossRef](#)]
25. Wanjara, P.; Jahazi, M.; Monajati, H.; Yue, S.; Immarigeon, J.P. Hot working behavior of near-alpha alloy IMI834. *Mater. Sci. Eng. A* **2005**, *396*, 50–60. [[CrossRef](#)]
26. Ebrahimi, R.; Najafizadeh, A. A new method for evaluation of friction in bulk metal forming. *J. Mater. Process. Technol.* **2004**, *152*, 136–143. [[CrossRef](#)]
27. Gholamadeh, A.; Taheri, A.K. The prediction of hot flow behavior of Al-6%Mg alloy. *Mech. Res. Commun.* **2009**, *36*, 252–259. [[CrossRef](#)]
28. Roebuck, B.; Lord, J.D.; Brooks, M.; Loveday, M.S.; Sellars, C.M.; Evans, R.W. Measurement of flow stress in hot axisymmetric compression tests. *Mater. High Temp.* **2006**, *23*, 59–83. [[CrossRef](#)]
29. Shafaat, M.A.; Omidvar, H.; Fallah, B. Prediction of hot compression flow curves of Ti-6Al-4V alloy in alpha plus beta phase region. *Mater. Des.* **2011**, *32*, 4689–4695. [[CrossRef](#)]
30. Mirzadeh, H. Constitutive analysis of Mg-Al-Zn magnesium alloys during hot deformation. *Mech. Mater.* **2014**, *77*, 80–85. [[CrossRef](#)]
31. Mandal, S.; Rakesh, V.; Sivaprasad, P.V.; Venugopal, S.; Kasiviswanathan, K.V. Constitutive equations to predict high temperature flow stress in a Ti-modified austenitic stainless steel. *Mater. Sci. Eng. A* **2009**, *500*, 114–121. [[CrossRef](#)]
32. Haghdadi, N.; Zarei-Hanzaki, A.; Abedi, H.R. The flow behavior modeling of cast A356 aluminum alloy at elevated temperatures considering the effect of strain. *Mater. Sci. Eng. A* **2012**, *535*, 252–257. [[CrossRef](#)]

